Systematic Model Selection for Grey Box Modeling of HVAC Systems

V. Seiler[1*], G. Huber[1], P. Kepplinger[1]

[1]Illwerke vkw Endowed Professorship for Energy Efficiency, Research Center Energy,
Josef Ressel Centre for Intelligent Thermal Energy Systems,
Vorarlberg University of Applied Sciences, Hochschulstraße 1, 6850 Dornbirn, Austria

*Corresponding author: valentin.seiler@fhv.at

Abstract

Grey Box models provide an important approach for control analysis in the Heating, Ventilation and Air Conditioning (HVAC) sector. Grey Box models consist of physical models where parameters are estimated from data. Due to the vast amount of component models that can be found in literature, the question arises, which component models perform best on a given system or dataset? This question is investigated systematically using a test case system with real operational data. The test case system consists of a HVAC system containing an energy recovery unit (ER), a heating coil (HC) and a cooling coil (CC). For each component, several suitable model variants from the literature are adapted appropriately and implemented. Four model variants are implemented for the ER and five model variants each for the HC and CC. Further, three global optimization algorithms and four local optimization algorithms to solve the nonlinear least squares system identification are implemented, leading to a total of 700 combinations. The comparison of all variants shows that the global optimization algorithms do not provide significantly better solutions. Their runtimes are significantly higher. Analysis of the models shows a dependency of the model accuracy on the number of total parameters.

Keywords: Grey Box, Modeling, HVAC, Model selection

Introduction

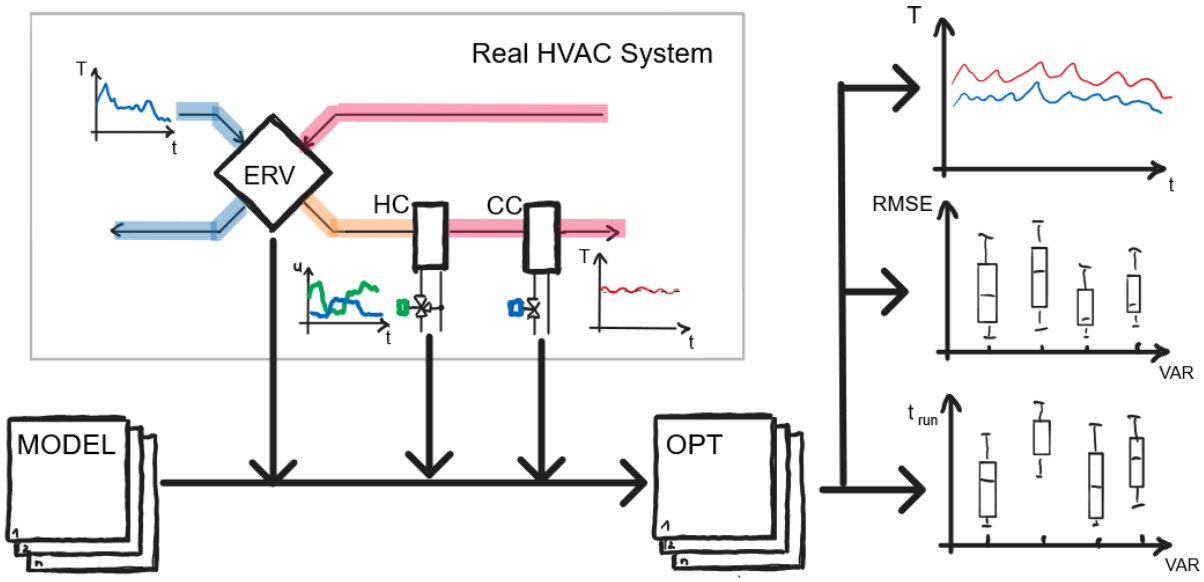

Figure 1. Scheme of the Model Selection

Grey Box modeling of Heating, Ventilation and Air Conditioning (HVAC) systems is used for control analysis and set point optimization [1, 2] and, therefore, provides an important pillar

for efficient system operation. Grey Box models are created by formulating physical (White Box) models and estimating unknown parameters from recorded data of the real system. This parameter estimation is done through nonlinear optimization, e.g., nonlinear least squares [3]. In contrast to Black Box models (also known as data-driven models) and White Box models, being the other common modeling approaches, Grey Box models are reported to have the following benefits [4, 1]:

- usually better generalization capability than Black Box models;
- lower data quality necessary than Black Box models;
- better accuracy possible than White Box models.

In literature, examples for the modeling of HVAC systems with the Grey Box approach can be found and will be outlined in the following.

Afram and Janabi-Sharifi [4] and Afroz et al. [1] review modelling methods in HVAC sector. As part of their analysis, they present common component models. Also, Okochi and Yao [5] present a review of variable-air-volume air-conditioning systems, which also includes component models.
Ghiaus, Chicinas, and Inard [6] performed a Grey Box identification of elements of ventilation systems. Here, the system consists of two electric heating coils (one for preheating and one for heating), a cooling coil, and an evaporator for air humidification. The relative humidity and the temperature of the supply air are controlled. The system is divided into small Single Input Single Output (SISO) elements, which are identified independently. A damped Gauss-Newton algorithm is used to identify the Grey Box parameters.
Koehler et al. [7] create a simple Grey Box model of a ventilation system for use in model predictive control.
Very detailed modeling of an entire HVAC system of a prototype residential building using the Grey Box approach is presented by Afram and Janabi-Sharifi [8]. Among the components considered is the ventilation system with heat recovery and cooling coil. Nonlinear least squares optimization is used to find the parameters of the models.

Systems under consideration generally consist of the same principal components including heating coils (HC), cooling coils (CC), mixing boxes (MB), energy recovery units (ER), humidifiers, ductwork, dampers and valves. Further, components of the energy supply side like heat pumps, buffer tanks and cooling towers as well as the building zones are commonly modeled.

Very little justification is given on how each model type is selected for each component, especially, as there is a great variety of model variants. Particularly for the heat exchanger modeling of ER, HC and CC units, several variations can be found and shall shortly be presented. Common steady state models are based on the so-called Number of Transfer Unit (NTU) approach [9]. Modeling examples can be found in [10, 5, 1] and it is also used in the simulation software TRNSYS® [11] as a simplified model. There, either a constant effectiveness ϵ or a correlation, to determine the effectiveness, is used. Various correlations for different heat exchangers exist, basic correlations can be found in [9], and advanced correlations for air-coils can be found for example in [12]. Dynamic models, mapping time-dependent or capacitive effects, are commonly used for control analysis. Chen and Treado [13] use a model which includes a time constant into the NTU approach, making it dynamic. Other models use simple energy balances over the heat exchanger, either using one thermal mass (for example presented in [14]) or two thermal masses (used by [8]). Those models generally map heat transfer in a simplified manner.

When it comes to a real system, the question one is confronted with is: Which of the given models performs best for the given system and dataset? To do a systematic evaluation, we

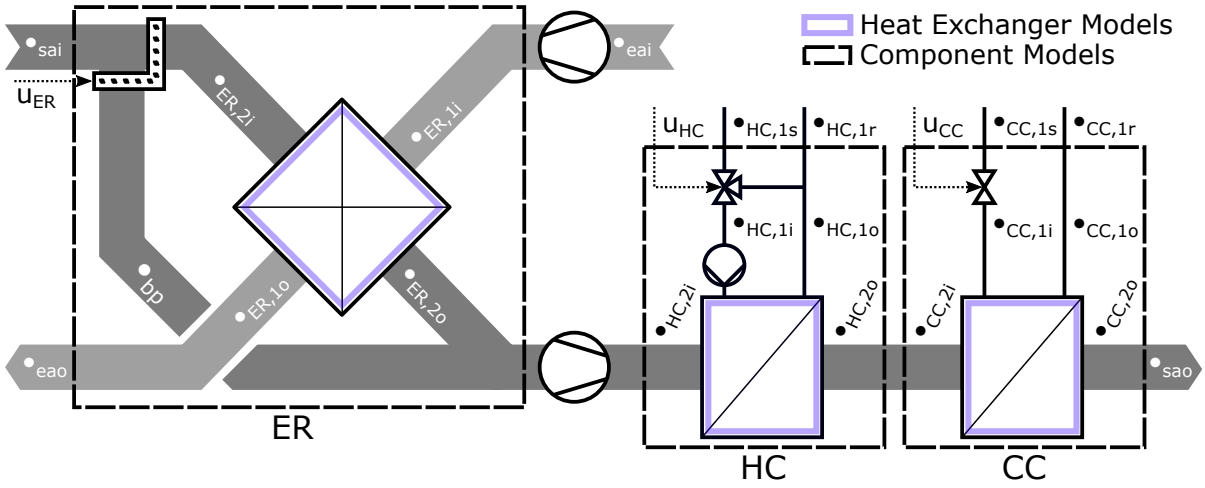

Figure 2. Scheme of the showcase ventilation system. The symbols represent the following: ER - Energy Recovery, HC - Heating Coil, CC - Cooling Coil, sa - supply air, ea - exhaust air, i - in, o - out, s - supply, r - return, bp - bypass and u - control signal

propose a grid search model selection, where suitable models are compared with each other. We present the approach based on a showcase system using real operational data with limited sensor and data availability. The principal methodology can be seen in Figure 1. Suitable model variants are selected representing the above-stated different heat exchanger formulations. Four variants for the ER, five variants of the HC and five variants of the CC are implemented, resulting in a total of 100 model combinations. Furthermore, a comparison of seven different optimization algorithms for system identification (solving the nonlinear least squares problem) is presented on all model variants, leading to a total of 700 combinations evaluated.

Methods

At first, a short description on how the overall grid search is performed on the given system is presented. Then all model variants are presented in detail, starting with general heat exchanger models, followed by the description of the particular component models that are based on the general heat exchanger models. Eventually, the system identification using the nonlinear least squares is described.

The system, subject of this project, is a ventilation system of a salesroom, where several months of recorded operating data is available. It is depicted in Figure 2. Modeling in this particular case is done, to create a test field to improve the temperature controller for the conditioned air. The components that need to be modeled are the ER, the HC, and the CC. The two fans are not modeled as they provide constant airflow, and, are irrelevant for the controller analysis. Therefore, all components are heat exchangers in different configurations. For each component, several models were identified from the literature and are adapted, to be applied to this system.

The project is implemented in Python as it provides good capabilities in data preprocessing, data analysis and optimization. In general, the system identification process developed in this project consists of three steps:

1. A combination of component models is selected.
2. An optimization algorithm is selected.
3. The model parameters are optimized (identified) by solving the nonlinear least squares problem with the chosen optimization algorithm.

Component models will be presented, starting with principal heat exchanger models, which provide the basis of the components modeled

A simplified model using the so-called effectiveness - NTU method [9] is, for example, used for modeling by Schito [10], Okochi and Yao [5], and Afroz et al. [1], and is also used in the simulation software TRNSYS® [11] as a simplified heat exchanger model. The basis of the method is that a fraction, ϵ, of the maximum transferable heat flow is transferred from the hot fluid to the cold fluid. In theory, the maximum transferable heat flow is obtained in a counter-flow heat exchanger of infinite length. Here, the temperature of the fluid with the smaller heat capacity would take on the input temperature of the fluid with the larger heat capacity [9]. The heat capacity flows $\dot{C}$ of each fluid 1 and 2 of the heat exchanger are calculated by $\dot{C}_1 = c_{\mathrm{p1}}\dot{m}_1$ and $\dot{C}_2 = c_{\mathrm{p2}}\dot{m}_2$, where c_{pn} denotes the specific heat capacity and $\dot{m}_n$ denotes the mass flow of fluid n. With $\dot{C}_{\max} = \max(\dot{C}_1, \dot{C}_2)$ and $\dot{C}_{\min} = \min(\dot{C}_1, \dot{C}_2)$, the maximum transferable heat can be calculated by

$$\dot{Q}_{\max} = \dot{C}_{\min}(T_{1\mathrm{i}} - T_{2\mathrm{i}}). \tag{1}$$

The temperatures at the outputs are then given by

$$T_{1\mathrm{o}} = T_{1\mathrm{i}} + \frac{\epsilon \dot{Q}_{\max}}{\dot{m}_1 c_{\mathrm{p1}}} \text{ and} \tag{2}$$

$$T_{2\mathrm{o}} = T_{2\mathrm{i}} - \frac{\epsilon \dot{Q}_{\max}}{\dot{m}_2 c_{\mathrm{p2}}}, \tag{3}$$

where indices i and o refer to in and out. Due to [9], the effectiveness ϵ can be calculated as an analytical expression for all heat exchanger types as a function $\epsilon = f\,(NTU, C_{\mathrm{r}})$. Here, $C_{\mathrm{r}} = \frac{\dot{C}_{\min}}{\dot{C}_{\max}}$ and the NTU is a dimensionless ratio widely used in heat exchanger analysis. It is defined according to [9] as $NTU = \frac{UA}{\dot{C}_{\min}}$, where U is the heat transfer coefficient in W/K and A is the area in m^2 of the heat exchanger. Many ϵ correlations for common heat exchanger types can be found in the literature. For the ER, the following correlation is implemented according to [9], assuming that the heat exchanger is a cross-flow type:

$$\epsilon = 1 - e^{\frac{1}{C_{\mathrm{r}}}(NTU)^{0.22}\left(e^{-C_{\mathrm{r}}(NTU)^{0.78}}-1\right)}. \tag{4}$$

Detailed ϵ correlations for air coils can be found in [12], for example. However, here we implement an ϵ-correlation for counter flow heat exchangers for the HC and the CC according to [9], as a general assumption, as the exact design of the coil is unknown:

$$\epsilon = \frac{1 - e^{-NTU(1-C_{\mathrm{r}})}}{1 - C_{\mathrm{r}} e^{-NTU(1-C_{\mathrm{r}})}} \qquad \text{for} \quad C_{\mathrm{r}} < 1 \tag{5}$$

$$\epsilon = \frac{NTU}{1 + NTU} \qquad \text{for} \quad C_{\mathrm{r}} = 1. \tag{6}$$

However, this NTU method only maps the steady state. Chen and Treado [13] use a heating coil model, that is also based on the $\epsilon - NTU$ method, but models the capacitive dynamics of the coil. In the following, this variant will be referred to as *NTU Dyn*. Here, the equilibrium temperatures are also calculated according to equation (2) and (3). Whereby the dynamic temperatures are additionally calculated by

$$\frac{\mathrm{d}T_{1\mathrm{o,dyn}}}{\mathrm{d}t} = \frac{T_{1\mathrm{o}} - T_{1\mathrm{o,dyn}}}{\tau} \text{ and} \tag{7}$$

$$\frac{\mathrm{d}T_{2\mathrm{o,dyn}}}{\mathrm{d}t} = \frac{T_{2\mathrm{o}} - T_{2\mathrm{o,dyn}}}{\tau}. \tag{8}$$

According to Chen and Treado, the time constant τ is composed of a capacitive term τ_c and a "flush time" τ_x as $\tau = \frac{1}{\tau_c^{-1}+\tau_x^{-1}}$. In this paper, however, τ is identified as a single parameter in the system identification.

Another modeling approach is for example used by [14], which will be referred to as *UA1C*-method hereafter. The heat exchanger is modeled using a single energy balance as follows:

$$\frac{\mathrm{d}T_{1o}}{\mathrm{d}t} = \frac{1}{C}\left[\dot{m}_2 c_{p2}(T_{2i} - T_{2o}) + UA(T_{env} - T_{1o}) - \dot{m}_1 c_{p1}(T_{1i} - T_{1o})\right]. \tag{9}$$

Where T_{env} is the environment temperature. If the heat exchange with the environment $UA(T_{env} - T_{1o})$ is neglected, Equation (9) becomes

$$C\frac{\mathrm{d}T_{1o}}{\mathrm{d}t} = \dot{m}_2 c_{p2}(T_{2i} - T_{2o}) - \dot{m}_1 c_{p1}(T_{1i} - T_{1o}). \tag{10}$$

From Tashtoush, Molhim, and Al-Rousan [14] it is assumed that the return temperature of fluid 2 is constant $T_{2o} = 10°\mathrm{C}$, since this temperature is not a model output, unlike in the other model variants. In this paper, T_{2o} is included as a parameter for system identification.

Another approach using two coupled energy balance equations, one for each fluid, can be found in a paper by Afram and Janabi-Sharifi [8]. This method is referred to as *UA2C* hereafter. The ER model is formulated as such, following [8]:

$$\frac{\mathrm{d}T_{1o}}{\mathrm{d}t} = \frac{1}{C_{am}}\left[\dot{m}_1 c_{p1}(T_{1i} - T_{1o}) - UA\left(\frac{T_{1i}+T_{1o}}{2} - \frac{T_{2i}+T_{2o}}{2}\right)\right] + c_1 \tag{11}$$

$$\frac{\mathrm{d}T_{2o}}{\mathrm{d}t} = \frac{1}{C_{am}}\left[UA\left(\frac{T_{1i}+T_{1o}}{2} - \frac{T_{2i}+T_{2o}}{2}\right) - \dot{m}_2 c_{p2}(T_{2o} - T_{2i})\right] + c_2. \tag{12}$$

C_{am} is the heat capacity of the air and metal in the heat exchanger. Here, C_{am}, UA, c_1 and c_2 are identified in the system identification where parameters c_1 and c_2 represent correction terms intended to compensate for modeling inaccuracies. This variant is implemented in two separate sub-variants, once using the correction terms (named *UA2C c*) and, once, without correction terms to study their influence. Afram and Janabi-Sharifi [8] also present a model for an air handling unit (here equivalent to a cooling coil) model similar to their ER model. Here, heat transfer is characterized by the term $UA(T_{1o} - T_{2o})$ unlike with the ER model. Thus, the differential equations are as follows:

$$\frac{\mathrm{d}T_{1o}}{\mathrm{d}t} = \frac{1}{C_1}\left[\dot{m}_1 c_{p1}(T_{1i} - T_{1o}) - UA(T_{1o} - T_{2o})\right] + c_1 \tag{13}$$

$$\frac{\mathrm{d}T_{2o}}{\mathrm{d}t} = \frac{1}{C_2}\left[UA(T_{1o} - T_{2o}) - \dot{m}_2 c_{p2}(T_{2o} - T_{2i})\right] + c_2. \tag{14}$$

With $C_2 = 1 * c_{p2}$, all other parameters are identical to the ER model stated before. Here again, it is implemented in two separate sub-variants with and without correction terms c_1 and c_2.

These mentioned heat exchanger models are then adapted accordingly to fit the test case system. Therefore, power control for each component needs to be modeled. The ER is equipped with a bypass for power control as can be seen in Figure 2. The bypass diverts a part of the air stream around the heat exchanger to control the recovered power. Under the assumption of linear valve behavior, the two air streams after the valve can be modeled as

$$\dot{m}_{ER,2} = \dot{m}_{sai}\, u_{ER} \text{ and} \tag{15}$$

$$\dot{m}_{bp} = \dot{m}_{sai}\,(1 - u). \tag{16}$$

Where $\dot{m}_{\mathrm{bp}}$ denotes the air stream through the bypass, $\dot{m}_{\mathrm{ER},2}$ denotes the air stream through the heat exchanger, $\dot{m}_{\mathrm{sai}}$ denotes the total supply airflow into the ER and u_{ER} denotes the control signal for the three-way valve of the ER. Note, that the notation here is following Figure 2. The mixing temperature at the ER outlet (HC inlet), assuming a constant specific heat capacity of the air, is obtained from the energy balance by

$$T_{\mathrm{HC,2i}} = T_{\mathrm{ER,2o}} u_{\mathrm{ER}} + T_{\mathrm{sai}}(1 - u_{\mathrm{ER}}). \tag{17}$$

For the heat exchanger of the ER, four of the above-mentioned models were used: *NTU, NTU Dyn, UA2C, UA2Cc*. The *UA1C* model was excluded due to expected low performance. The fluid flows 1 and 2 of the heat exchanger models correspond to the exhaust and supply air, respectively.

Similar to the energy recovery, the heating coil is composed of two subcomponents, the water-air heat exchanger and a three-way valve, which controls the power of the coil. The mass flow in the heat exchanger itself is constant and, depending on the valve position, water from the return is proportionally added to the flow through the heat exchanger. The constant mass flow $\dot{m}_{\mathrm{HC,1}}$ can be determined as a parameter of the model during system identification. The temperature at the inlet of the heat exchanger is therefore formed as a mixed temperature from the supply temperature and the return temperature of the heat exchanger. From the energy balance of the three-way valve follows for the mixed temperature $T_{\mathrm{HC,1i}}$ depending on the control input u_{HR} of the valve:

$$T_{\mathrm{HC,1i}} = T_{\mathrm{HC,1s}} u_{\mathrm{HC}} + T_{\mathrm{HC,1o}}(1 - u_{\mathrm{HC}}). \tag{18}$$

For the water-to-air heat exchanger, all five of the above-described variants from the literature were implemented. Fluids 1 and 2 of the heat exchanger models refer to water and air respectively.

The cooling coil power is controlled via a valve to control the power output. Different from the heating coil, this is done with a throttle valve. Therefore, under the assumption of linearity of the valve $u_{\mathrm{CC}} \sim \dot{m}_{\mathrm{CC,1i}}$, the equation for the mass flow can be formulated as follows:

$$\dot{m}_{\mathrm{CC,1i}} = u_{\mathrm{CC}} \cdot \dot{m}_{\mathrm{1,max}}. \tag{19}$$

Here the maximum mass-flow $\dot{m}_{\mathrm{1,max}}$ can be determined as a parameter during system identification. To model the water-to-air heat exchanger, the same variants can be used as in the heating coil. This modeling implies, that there is no condensation taking place during the cooling process.

All used model variants for each component, including their start parameters and bounds for the optimization, are shown in Table 1.

Since the components have no feedback within the system boundaries, they can be solved independently. Thus, the first component of the model forms the input of the second component and the second the input of the third. All components are transformed into general time-discrete input-output models with a time resolution of one minute in the following form:

$$y_i^* = f(y_{i-1}^*, x_i). \tag{20}$$

Where y_i^* is the output vector of model f at time i, y_{i-1}^* is the model output vector at time $i-1$ and x_i is the model input vector at time i. To get all models into the given form, differential equations need to be solved. The solution of the differential equations is obtained analytically. Models containing coupled systems of differential equations are solved, by transformation into

Table 1. Component Models

Component	Model	Parameter	Start value	lb	ub	Unit
ER	NTU	UA	3933.9	1	5000	W/K
	NTU Dyn	UA	3933.9	1	5000	W/K
		τ	60	1	500	s
	UA2C	UA	3933.9	1	5000	W/K
		C_{am}	25000.0	1	500000	J/K
	UA2C c	UA	3933.9	1	5000	W/K
		C_{am}	25000.0	1	500000	J/K
		c_1	0	-10	10	
		c_2	0	-10	10	
HC	NTU	$\dot{m}_{\mathrm{HC},1}$	0.2908	0.1	5	kg/s
		UA	258.76	1	5000	W/K
	NTU Dyn	$\dot{m}_{\mathrm{HC},1}$	0.2908	0.1	5	kg/s
		UA	258.76	1	5000	W/K
		τ	60	1	500	s
	UA1C	$\dot{m}_{\mathrm{HC},1}$	0.2908	0.1	5	kg/s
		C	500000	1	500000	J/K
		$T_{1\mathrm{o}}$	40.0	1	70	°C
	UA2C	$\dot{m}_{\mathrm{HC},1}$	0.2908	0.1	5	kg/s
		UA	258.76	1	5000	W/K
		C_{wm}	250000	1	500000	J/K
	UA2C c	$\dot{m}_{\mathrm{HC},1}$	0.2908	0.1	5	kg/s
		UA	258.76	1	5000	W/K
		$\dot{m}_{\mathrm{HC},1}$	250000	1	500000	J/K
		c_1	0	-10	10	
		c_2	0	-10	10	
CC	NTU	$\dot{m}_{1,\mathrm{max}}$	0.4625	0.1	5	kg/s
		UA	1485.2	1	5000	W/K
	NTU Dyn	$\dot{m}_{1,\mathrm{max}}$	0.4625	0.1	5	kg/s
		UA	1485.2	1	5000	W/K
		τ	60	1	500	s
	UA1C	$\dot{m}_{1,\mathrm{max}}$	0.4625	0.1	5	kg/s
		C	500000	1	500000	J/K
		$T_{1\mathrm{o}}$	18.0	1	20	°C
	UA2C	$\dot{m}_{1,\mathrm{max}}$	0.4625	0.1	5	kg/s
		UA	1485.2	1	5000	W/K
		C_{wm}	250000	1	500000	J/K
	UA2C c	$\dot{m}_{1,\mathrm{max}}$	0.4625	0.1	5	kg/s
		UA	1485.2	1	5000	W/K
		C_{wm}	250000	1	500000	J/K
		c_1	0	-10	10	
		c_2	0	-10	10	

their eigenbasis. The heating coil, where the return temperature is at the same time its input temperature, requires the models to be solved iteratively for each time step.

The parameters of the models are identified using optimization technics. This optimization aims to minimize the error between the model output and the dataset. In the presented test case, there are two model outputs with corresponding measurements in the dataset. Therefore, the calculated error is the sum of the individual errors of each model output and the minimization can be formulated as

$$\min_{p} \sum_{i \in \mathcal{I}} \left((y^*_{1,i}(p) - y_{1,i})^2 + (y^*_{2,i}(p) - y_{2,i})^2 \right) \tag{21}$$

$$s.t.\ lb \leq p \leq ub. \tag{22}$$

Where $y^*_{1,i}(p)$ and $y^*_{2,i}(p)$ are the outputs of a model at time i with the parameter-vector p. $y_{1,i}$ and $y_{2,i}$ are the corresponding measurements from the dataset at the same time and lb and ub are the lower and upper bounds for the parameter vector p. Values for the upper and lower bound of each parameter are given in Table 1. For the optimization, the parameters p are scaled logarithmically. The algorithms require an initial guess for the parameters p as a starting point for the optimization (start parameters). These values were taken from the data sheet of the system if available. They are also given in Table 1.

For the optimization algorithms, the choice was made from a selection of global and local optimization algorithms available in the Python SciPy library [15, 16] which provides a selection of common optimization routines. The selection criteria were, that the algorithm has to accept bounds and no derivatives are needed. Furthermore, some algorithms were excluded due to unreasonable long runtimes based on a preliminary study. The selected local optimization algorithms are:

- Nelder-Mead
- L-BFGS-B
- Powell
- TNC

The global optimization algorithms are:

- Differential-Evolution
- Dual-Annealing
- DIRECT

Data for the system identification was extracted from the control unit of the showcase system over several months. Relevant measurement points of the system are displayed in Table 2. T_{sao} and $T_{\mathrm{HC,1r}}$ correspond to outputs of the model and can therefore be used to formulate the error function of the optimization (Equation (21)). However, not all outputs of the model are represented in the dataset, which means they cannot be used in the error calculation. Intermediate measurements of the supply air are, for example, not available which is assumed to limit the accuracy of the model variants. Further, the measurements of the plant are taken in irregular time steps, based on a constant delta. To mimic this behavior in the model, a sensor model is implemented. Also, the data needs to be pre-processed. This preprocessing is done by resampling the irregularly sampled dataset to a one-minute time resolution for usability in the time discrete model. Further, suitable days, when model assumptions hold, and no faulty behavior is detected in the dataset are selected based on formulated conditions, systematically. Further details on the data preprocessing can be found in [17].

Table 2. Measurements of the test case system

Position	Quantity	Unit	Symbol
Supply air	Mass flow	kg/s	$\dot{m}_{\mathrm{sa}}$
Supply air in	Temperature	°C	T_{sai}
Supply air out	Temperature	°C	T_{sao}
Return air	Mass flow	kg/s	$\dot{m}_{\mathrm{ra}}$
Return air in	Temperature	°C	T_{rai}
Heating coil supply	Temperature	°C	$T_{\mathrm{HC,1s}}$
Heating coil return	Temperature	°C	$T_{\mathrm{HC,1r}}$
Cooling coil supply	Temperature	°C	$T_{\mathrm{CC,1s}}$
Controller	Output		u_{ER}, u_{HC}, u_{CC}

The available dataset starts on 03/03/2022 and ends on 08/06/2022, thus containing 98 days. After applying the preprocessing rules, only eight days show to be suitable for system identification. Then a training- and a test dataset are selected from the suitable days for parameter identification and model verification respectively. The outdoor temperature provides a good indication of the operating state of the plant. The training and test data sets each contain a range of outdoor temperatures from about 0°C to just over 30°C. However, the distributions are different, so the extrapolation ability of the model can be verified by the test data set.

Results

The model outputs, T^*_{sao} and $T^*_{\mathrm{HC,1r}}$ of the model with the lowest error can be seen in Figure 3. They are plotted against the corresponding measurements T_{sao} and $T_{\mathrm{HC,1r}}$. Both outputs capture the general swinging dynamics of the system, noting, that the swinging dynamics are already present in the controller output of the dataset. The deviation is mostly (90% of time) below 1.6 K for T_{sao} and below 3.7 K for $T_{\mathrm{HC,1r}}$, however, still significant.

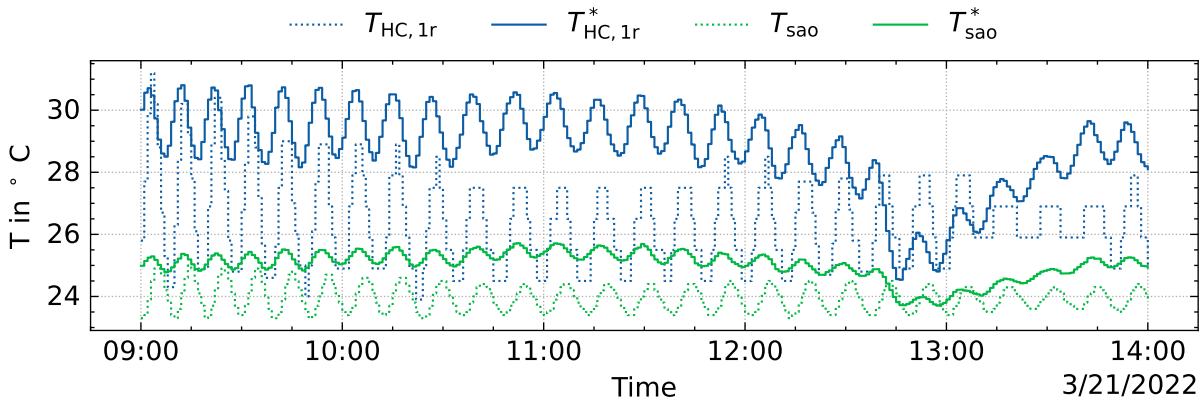

Figure 3. Exemplary model output ($T^*_{\mathrm{HC,1r}}$, T^*_{sao}) and corresponding measurements ($T_{\mathrm{HC,1r}}$, T_{sao})

Calculated performance metrics of the final model (on training and test data) can be seen in Table 3. Notably, the metrics are comparably worse than other Grey Box modeling approaches, for example Afram and Janabi-Sharifi [8], who reach RMSEs between 0.224 and 1.127, however, for individual component models.

The grid search approach, applied to the test case system, yields a total of 700 combinations of models and optimization algorithms. The test dataset is primarily used, to test the extrapolation

Table 3. Metrics of the final model.

		$T_{\mathrm{HC,1r,train}}$	$T_{\mathrm{HC,1r,test}}$	$T_{\mathrm{sao,train}}$	$T_{\mathrm{sao,test}}$
RMSE	Root Mean Square Error	2.377	2.320	1.050	1.281
R^2	Coefficient of multiple determination	0.992	0.992	0.998	0.997
MSE	Mean Squared Error	5.650	5.381	1.102	1.642
MAE	Mean Absolute Error	1.603	1.430	0.831	0.931

ability of the models or the overfitting tendency of the models. This is done by comparing the achieved errors of the training and test dataset. For analysis purposes, the RMSE (Root Mean Squared Error) of each model is used. Figure 4 shows the division of the RMSE of the training dataset divided by the RMSE of the test dataset. A value smaller than one indicates, that the model performs better on the training dataset than on the test dataset, which indicates a low extrapolation ability or overfitting. Values greater than one indicate, that the model performs better on the test dataset, which can be coincidental. Plot 1 of Figure 4 shows the sum of the errors of both model outputs (T_{sao} and $T_{\mathrm{HC,1r}}$). As the values are close to one, overfitting appears to be insignificant. However, the second and the third plots show, that the RMSE of T_{sao} tends to overfit more significantly, which seems to be compensated by the RMSE of $T_{\mathrm{HC,1r}}$.

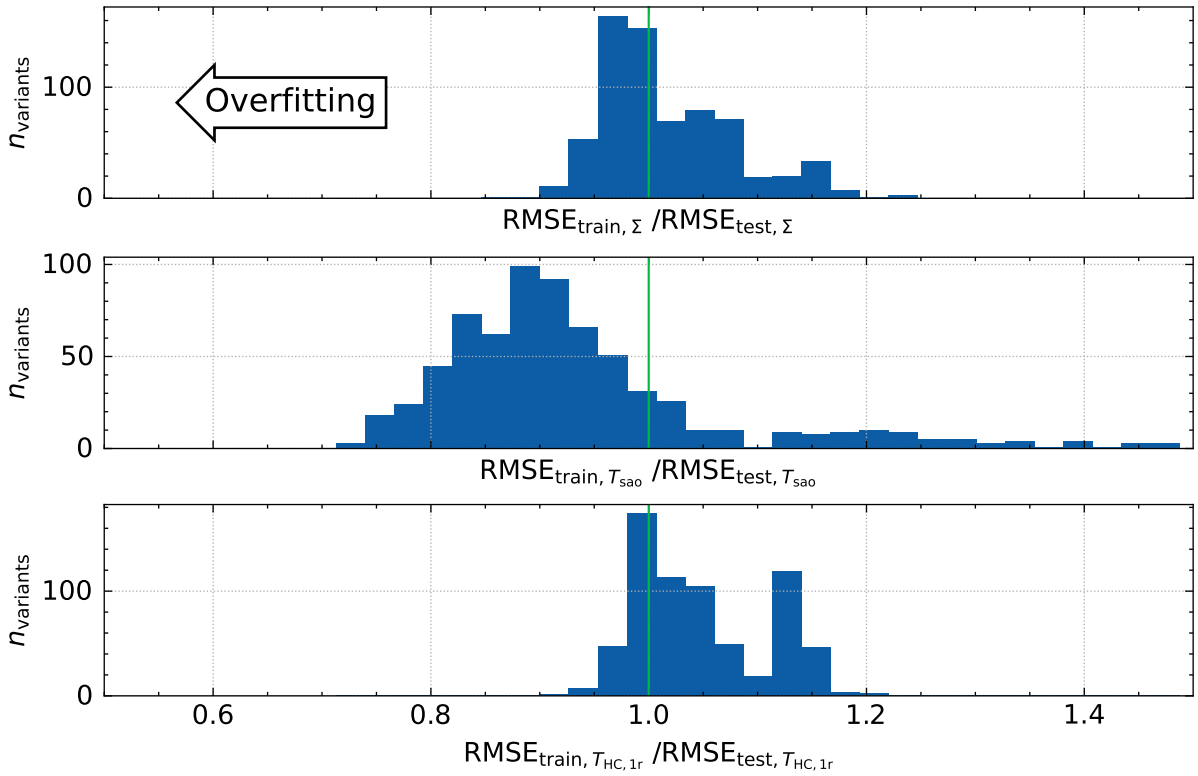

Figure 4. Histogram of the ratios of the $\mathrm{RMSE}_{\mathrm{train}}/\mathrm{RMSE}_{\mathrm{test}}$ of all 700 model variants, which provide an indicator for overfitting. Plot 1 shows the ratio for the summed errors of both model outputs. Plot 2 shows the ratio for the error of T_{sao}, and plot 3 for $T_{\mathrm{HC,1r}}$.

Figure 5 shows the comparison of the optimization algorithms. Again, the RMSE is used for evaluation. Note, that some algorithms did not converge, however, the results are included, as long as they were returned by the algorithm. As can be seen, the distributions of all optimization algorithms have similar minimum and maximum values except for some outliers of

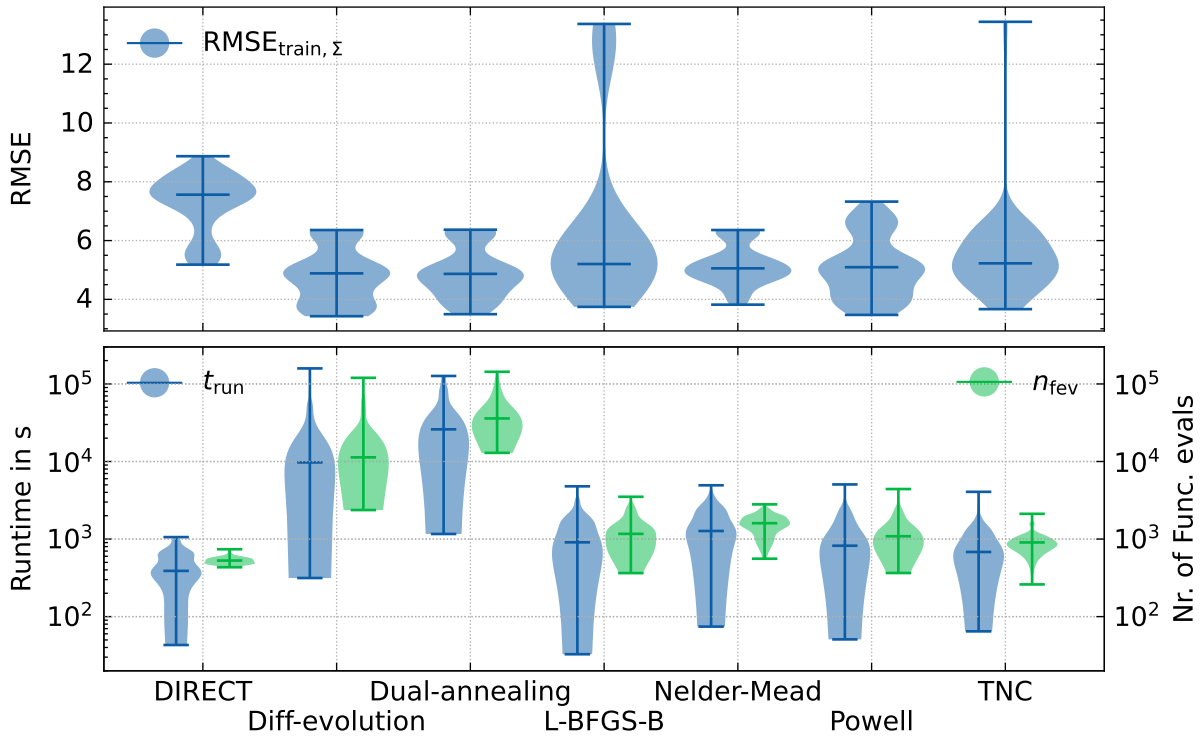

Figure 5. Comparison of performance of optimization algorithms in all 700 variants. Plot 1: Distributions of the sum of RMSE of T_{sao} and $T_{HC,1r}$ grouped by the optimization algorithm. Plot 2: Distribution of runtimes and the number of function evaluations grouped by the optimization algorithm.

the L-BFGS-B, the TNC algorithms, and the DIRECT method which performs worse in the optimization setting at hand. Further, the second plot shows that the global optimization algorithms Differential-Evolution and Dual-Annealing have significantly higher runtimes and more function evaluations compared to the local optimization algorithms. The global optimizer DIRECT also has lower runtimes and function evaluations. However, the achieved errors are, as mentioned, worse compared to the other algorithm.

Figure 6 shows an analysis grouped by the number of parameters. The first plot shows that with an increasing number of parameters, the mean absolute error decreases up to nine parameters. Then, the error does not decrease significantly with an increase in the number of parameters. The last plot shows that the median of the runtime for each optimization routine and the median of the number of function evaluations tend to increase with the number of parameters.

Discussion

The data selection process shows, that much of the recorded data does not fulfill the requirements for the model fit. This is mainly due to the low resolution and the resampling of the data. The low resolution is also expected to be the main cause of the comparably low model performance compared to results from the literature. A further cause for the low performance in the test case is the lack of intermediate measurements between the components, i.e., only the complete system can be identified as a whole in one process. In Figure 3, the drop in $T_{HC,1r}$ and T_{sao} at around 12:45 clearly shows that some effects are not represented in the dataset or that some dynamics are not modeled correctly. That shows the difficulties that arise with the usage of real operational data which is only addressed in literature very rarely.

One aspect to consider is, that the component models which are relevant, strongly depend on

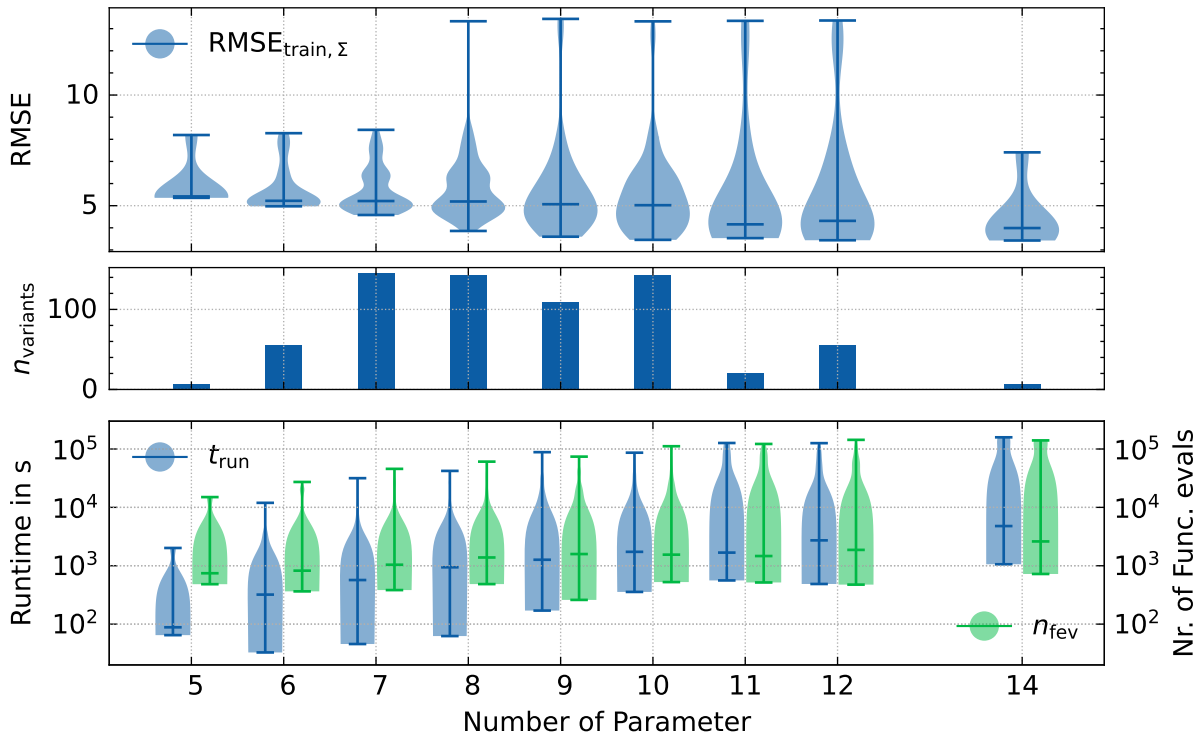

Figure 6. Analysis of sum of RMSE of T_{sao} and $T_{\text{HC,1r}}$, runtime and the number of function evaluations in dependency of the number of total model parameters. Note: There are more variants towards the middle of the spectrum as there are more possible component combinations with a given number of parameters, there is no possible combination of components that results in 13 parameters.

the later use case of the model. For example models for control analysis usually need to map capacitive effects, whereas quantitative energy analysis can usually cope with static models. Also, the time necessary for modeling, running system identification and evaluating several model variants for each component presents a significant drawback of the presented approach. This is especially the case, as there are no software solutions available for this kind of analysis. The lack of software solutions in modeling has already been addressed by [18].

However, interesting observations stem from the study results.

First, the runtime of the global optimizers is much longer than that of the local optimizers, the achieved model errors, however, do not show a significant difference in accuracy.

Secondly, the analysis of the number of parameters of the models shows that also simple models can yield results comparable to those of more complex modeling approaches.

Thirdly, the validation of the models with the test dataset shows, that some models tend to overfit on single outputs, whereas the overall error does not. This shows, that overfitting can be a relevant issue and, that the selection of the error function can be of great importance and multi-objective optimization should be considered.

Conclusions

In this project, a methodology for the selection of Grey Box models is presented on a real test case system. Therefore, several component models are identified for each component of the plant that needs to be modeled. Here, the energy recovery is modeled in four different variants and the heating coil and the cooling coil are each modeled in five different variants. For comparison, all possible model combinations are created and the parameters of the model are identified using four different local optimization algorithms and three global optimization algorithms. In total that leads to 700 system identifications.

The comparison of the optimization algorithms shows that the global optimizers have generally much longer runtimes and the achieved model errors are of comparable quality as those achieved by the local optimizers.

The analysis of different model variants shows that there is a dependency of the accuracy of the model and the number of parameters. Here, the achieved errors show a minimum at around nine parameters and the runtimes increase significantly with the number of parameters.

Further work should be done in evaluating the presented approach on different datasets with better quality to be able to make more general statements about suitable model types. A successive reduction in data quality, e.g., reducing the number of sensors and measurement intervals, could further yield results about necessary data quality for each type of model.

Even though the methodology provided probably renders to be too complex and time-consuming for most common modeling tasks, it can give insights into the system behavior and system identification process. Future works with Grey Box models should consider a systematic approach for system identification as this can help to determine the best-suited complexity of the model for a given system or dataset.

Acknowledgement

Part of this work has been published in [17].

The financial support by the Austrian Federal Ministry for Digital and Economic Affairs and the National Foundation for Research, Technology and Development, and the Christian Doppler Research Association are gratefully acknowledged.

References

[1] Zakia Afroz et al. "Modeling Techniques Used in Building HVAC Control Systems: A Review". In: *Renewable and Sustainable Energy Reviews* 83 (Mar. 2018), pp. 64–84. DOI: 10.1016/j.rser.2017.10.044.

[2] Mohammad Royapoor, Anu Antony, and Tony Roskilly. "A Review of Building Climate and Plant Controls, and a Survey of Industry Perspectives". In: *Energy and Buildings* 158 (Jan. 2018), pp. 453–465. DOI: 10.1016/j.enbuild.2017.10.022.

[3] Raad Z. Homod. "Review on the HVAC System Modeling Types and the Shortcomings of Their Application". In: *Journal of Energy* 2013 (2013), pp. 1–10. DOI: 10.1155/2013/768632.

[4] Abdul Afram and Farrokh Janabi-Sharifi. "Review of Modeling Methods for HVAC Systems". In: *Applied Thermal Engineering* 67.1-2 (June 2014), pp. 507–519. DOI: 10.1016/j.applthermaleng.2014.03.055.

[5] Godwine Swere Okochi and Ye Yao. "A Review of Recent Developments and Technological Advancements of Variable-Air-Volume (VAV) Air-Conditioning Systems". In: *Renewable and Sustainable Energy Reviews* 59 (June 2016), pp. 784–817. DOI: 10.1016/j.rser.2015.12.328.

[6] Christian Ghiaus, Adriana Chicinas, and Christian Inard. "Grey-Box Identification of Air-Handling Unit Elements". In: *Control Engineering Practice* 15.4 (Apr. 2007), pp. 421–433. DOI: 10.1016/j.conengprac.2006.08.005.

[7] Sarah M. Koehler et al. "Chapter 7 Distributed Model Predictive Control for Forced-Air Systems". In: *Intelligent Building Control Systems*. Ed. by John T. Wen and Sandipan Mishra. Advances in Industrial Control. Cham: Springer International Publishing, 2018. ISBN: 978-3-319-68461-1 978-3-319-68462-8. DOI: 10.1007/978-3-319-68462-8.

[8] Abdul Afram and Farrokh Janabi-Sharifi. "Gray-Box Modeling and Validation of Residential HVAC System for Control System Design". In: *Applied Energy* 137 (Jan. 2015), pp. 134–150. DOI: 10.1016/j.apenergy.2014.10.026.

[9] T. L. Bergman and Frank P. Incropera, eds. *Fundamentals of Heat and Mass Transfer*. 7th ed. Hoboken, NJ: Wiley, 2011. ISBN: 978-0-470-50197-9.

[10] Eva Schito. "Dynamic Simulation of an Air Handling Unit and Validation through Monitoring Data". In: *Energy Procedia* 148 (Aug. 2018), pp. 1206–1213. DOI: 10.1016/j.egypro.2018.08.010.

[11] S A Klein et al. *TRNSYS 16, Mathematical Reference*.

[12] Hélio Aparecido Navarro et al. "Effectiveness - NTU Data and Analysis for Air Conditioning and Refrigeration Air Coils". In: *Journal of the Brazilian Society of Mechanical Sciences and Engineering* 32.3 (Sept. 2010), pp. 218–226. DOI: 10.1590/S1678-58782010000300004.

[13] Yan Chen and Stephen Treado. "Development of a Simulation Platform Based on Dynamic Models for HVAC Control Analysis". In: *Energy and Buildings* 68 (Jan. 2014), pp. 376–386. DOI: 10.1016/j.enbuild.2013.09.016.

[14] Bourhan Tashtoush, M. Molhim, and M. Al-Rousan. "Dynamic Model of an HVAC System for Control Analysis". In: *Energy* 30.10 (July 2005), pp. 1729–1745. DOI: 10.1016/j.energy.2004.10.004.

[15] Pauli Virtanen et al. "SciPy 1.0: Fundamental Algorithms for Scientific Computing in Python". In: *Nature Methods* 17.3 (Mar. 2, 2020), pp. 261–272. DOI: 10.1038/s41592-019-0686-2.

[16] *Optimization and Root Finding (Scipy.Optimize) — SciPy v1.10.0 Manual*. URL: https://docs.scipy.org/doc/scipy/reference/optimize.html (visited on 01/06/2023).

[17] Valentin Seiler. *Grey-Box-Modellierung einer Lüftungsanlage mit realen Betriebsdaten für die Optimierung des Reglers*. 2022. DOI: 10.25924/opus-4580. URL: https://opus.fhv.at/frontdoor/index/index/docId/4580 (visited on 12/01/2022).

[18] Ercan Atam. "Current Software Barriers to Advanced Model-Based Control Design for Energy-Efficient Buildings". In: *Renewable and Sustainable Energy Reviews* 73 (June 2017), pp. 1031–1040. DOI: 10.1016/j.rser.2017.02.015.